



www.acsanm.org Article

Effects of Simulated Microgravity on the Internalization of Cerium Oxide Nanoparticles by Proliferating Human Skeletal Myoblasts

Giada Graziana Genchi,* Valentina Mollo, Matteo Battaglini, Melike Belenli Gümüş, Attilio Marino, Mirko Prato, Sergio Marras, Filippo Drago, Giammarino Pugliese, Francesca Santoro, and Gianni Ciofani*



Cite This: ACS Appl. Nano Mater. 2023, 6, 10853-10862



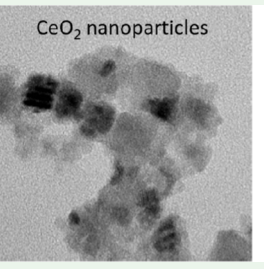
ACCESS

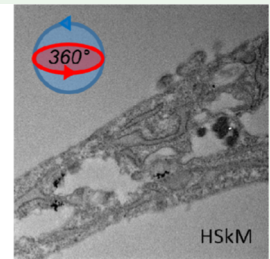
III Metrics & More



s Supporting Information

ABSTRACT: Spaceflight typically exerts detrimental effects on living organisms by promoting/accelerating some degenerative processes associated with aging and pathology onset on Earth, like muscle degeneration. As possible countermeasures to spaceflight effects, a few recent studies successfully tested the administration of nanomaterials for tuning of cellular activities and for promotion of certain cell phenotypes in microgravity, but largely missed investigation of early interactions of these nanomaterials with their cellular targets under altered gravity conditions. This study aims at filling this gap by elucidation of early interactions of a selected typology of redox-active nanoparticles (cerium oxide nanoparticles, also termed nano-





ceria, NC) with proliferating human skeletal myoblasts (HSkM) by concomitant exposure to simulated microgravity (achieved by a random positioning machine, RPM). To this purpose, NC were synthesized by a direct precipitation method and were chemically, structurally, and functionally characterized by several independent techniques prior to administration to skeletal muscle cell cultures and loading on the RPM. Confocal and electron microscopy evidence of nanoparticle internalization by several mechanisms (mostly involving macropinocytosis) in HSkM is provided, along with evidence of transcriptional regulation of key antioxidant response markers (Nos1, Sod2, and Sod3), promising oxidative stress alleviation and muscle protection under mechanical unloading conditions.

KEYWORDS: cerium oxide nanoparticles, human skeletal myoblasts, simulated microgravity, random positioning machine, nanoparticle internalization, transcriptional regulation

■ INTRODUCTION

Permanence in space is well known to detrimentally affect the astronauts' health, deteriorating their immune, musculoskeletal, and nervous systems, and leading to alterations very similar to those observed in the elderly due to the aging process. ^{1–3} Osteo- and sarcopenia are the most typical aging-like, pathological signs of gravitational unloading that severely impact on astronauts' motor function by very short-duration exposure, and that pose significant concerns for their entity, associated injury risks, and partial reversibility at return on Earth. ^{4,5} As traditional countermeasures to spaceflight-associated physiology alterations rely on food supplements and exercise with limited effectiveness, ^{6,7} novel approaches have very recently been proposed, making use of nanotechnology medicaments tested in both real and simulated microgravity (s-μg) conditions.

Administration of strontium-containing hydroxyapatite nanoparticles to human bone marrow mesenchymal stem cells was, for instance, studied for possible osteopenia treatment in different altered gravity conditions.⁸ Nanoparticles were supplied to cell cultures kept on board the International Space Station (ISS) and on a random positioning

machine (RPM), and effects of an 88 h interaction with the cells were investigated. Nanoparticle administration seemed to promote hydroxyapatite crystal deposition with respect to untreated cultures in real microgravity, whereas it supported alkaline phosphatase (ALP) activity retention in s-µg, thus promising applicability in bone tissue regeneration under critical environmental conditions. Again for bone tissue engineering purposes, a mixture of polymeric nanoparticles (poly-lactic acid and polyhydroxyalkanoate) loaded with bone morphogenetic proteins (2 and 7) was supplied to human adipose stem cells, demonstrating sustained and time-specific cargo release. Nanoparticle mixture promoted ALP activity, osteopontin expression, and transcription of selected osteodifferentiation marker genes in comparison to single nano-

Received: May 18, 2023 **Accepted:** May 23, 2023 **Published:** June 2, 2023





particle dispersions at 1g, and similar results were also achieved after a 2 h incubation with nanoparticles, followed by s- μg application for 20 days.⁹

Among the very few examples of nanomaterial applications to cell cultures under altered gravity conditions, there is the administration of cerium oxide nanoparticles (also termed nanoceria, NC) to both proliferating and differentiating skeletal muscle cells on board the ISS for possible sarcopenia treatment. In differentiating rat myoblasts, NC determined transcriptional regulation of genes involved in aging, body fat development, and mesodermal tissue proliferation, ¹⁰ whereas in proliferating mouse myoblasts, NC effects were overcome at the transcriptional level by spaceflight-induced ones, 11 leaving open questions and opportunities on NC application as a longlasting antioxidant agent against muscle wasting. Ground-based evidence encourages further investigations on NC muscleprotective role: intramuscular injections of NC improved muscle endurance in rats compared to untreated animals by increasing the muscle mass, glycogen, ATP production, type I fiber ratio, and mitochondriogenesis (in terms of organelle number and size). Proteomic analysis demonstrated that NCadministered, exercised rats showed increased oxidative phosphorylation, tricarboxylic acid cycle, and glycolysis products, as well as higher mitochondrial respiration and expression of electron-transport chain markers, compared to exercised-only rats. Inductively coupled plasma-mass spectrometry (ICP-MS) analysis on excised muscles revealed that nanoparticles were cleared by over 50% in 30 days and over 90% in 90 days from administration, with no evidence of inflammation or adverse effects. 12

This short literature review demonstrates that nanomaterial administration was conducted either prior to or at gravitational unloading of the selected biological models, thus leaving totally unexplored investigation of early interactions of nanoparticles with their targets *in vitro*. For this reason, this work aspired at clarifying short-term nanoparticle—cell interplay under s- μ g by evaluation of possible NC internalization and transcriptional effects at an early time point from administration under s- μ g. To the best of the authors' knowledge, this work reveals for the first time in the literature nanoparticle uptake under simulated microgravity and provides an insight on internalization and possible action modalities underlying NC effects on skeletal muscle cell cultures.

EXPERIMENTAL SECTION

Nanoparticle Synthesis. Cerium oxide nanoparticles were synthesized by ethylene glycol-assisted direct precipitation. Briefly, $Ce(NO_3)_3 \times 6H_2O$ (0.12 mol, 5.16 g) was dissolved in 8% (v/v) ethylene glycol in water (100 mL) and heated at 70 °C. Then, a 28–30% NH $_3$ OH solution in water was added dropwise under mild stirring until the pH became 9.2. After 1 h of incubation, nanoparticles were collected by five cycles of centrifugation (at 8000g for 20 min) and resuspension in water. Freeze-drying of an aliquot of nanoparticle dispersion was performed in order to quantify nanoparticles in the stock. Stabilization of the nanoparticles in aqueous medium was performed by incubating equal volumes of a 20 mg/mL NC dispersion in water and fetal bovine serum (FBS) under mild shaking for 1 h.

Nanoparticle Characterization. Transmission electron microscopy (TEM) was used to assess nanoparticle size immediately after synthesis (also after FBS coating), whereas Raman and X-ray photoelectron spectroscopy (XPS) were applied to investigate chemical composition. X-ray diffraction (XRD) was also used to confirm the chemical composition and characterize sample crystallinity. Thermogravimetric analysis was conducted to quantify the

extent of FBS adsorption on inorganic nanoparticles. Photometry was used to quantify nanoparticle total antioxidant capacity. Dynamic light scattering and Z-potential measurements were performed to assess colloidal stability of nanoparticle dispersions in aqueous media compatible to cell culture.

Transmission Electron Microscopy. TEM imaging was conducted on uncoated and FBS-coated nanoparticles by dispersion in ultrapure water at a final concentration of 1 mg/mL NC, and by dropping 50 μ L of dispersions onto carbon-coated copper grids. Imaging was performed in a bright-field modality with a Tecnai G2 F20 TWIN TMP transmission electron microscope set at 200 kV.

Raman Spectroscopy. Raman spectrum was collected by using a Horiba LabRAM HR Evolution Raman microscope equipped with a 532 nm laser and at a laser power of 10%. Nanoparticles were deposited on CaF_2 substrates, and Raman spectrum was obtained by averaging 15-point spectra. Acquisition was done with a $60\times$ immersion objective by three accumulations of 30 s each.

X-ray Photoelectron Spectroscopy. XPS analysis was performed on uncoated nanoparticles deposited onto an indium pellet with a Kratos Axis Ultra DLD spectrometer, equipped with a monochromatic Al K\$\alpha\$ source operating at 15 kV and 20 mA. A wide-scan spectrum was acquired with 160 eV pass energy, while a high-resolution narrow-scan spectrum was obtained with a constant 10 eV pass energy and steps of 0.1 eV. Photoelectrons were detected at a take-off angle $\varphi = 0^\circ$ with respect to the surface normal. The charging shift was calibrated with the binding energy of the C 1s as a baseline (284.8 eV). Data were acquired at a pressure lower than $7 \cdot 10^{-9}$ Torr in the analysis chamber, and they were converted to VAMAS format and processed using the CasaXPS 2.3.22 software.

X-ray Diffraction. XRD analysis was performed on uncoated nanoparticles with a Rigaku SmartLab X-ray powder diffractometer, equipped with a 9 kW Cu K α rotating anode operating at 40 kV and 150 mA, a D/teX Ultra 1D silicon strip detector, and a five-axis goniometer. The diffraction pattern was collected in Bragg—Brentano geometry over an angular range $2\theta=20-100^\circ$, with a step size of 0.02° . The measurement was carried out at room temperature by using a zero-diffraction silicon substrate. Size-strain analysis was carried out using the whole-powder-pattern decomposition technique based on the Pawley algorithm. Fundamental parameter profile fitting was used to simulate the instrument contribution. All parameters were refined by the least-squares method by using the Rigaku PDXL 2.8.1.1 software.

Thermal Gravimetric Analysis. Thermal gravimetric analysis (TGA) was conducted with a TA instruments Q500 thermal analyzer under a 50 mL/min nitrogen flux on \sim 5 mg of nanoparticle powders, obtained by lyophilization of 1 mL of both uncoated and FBS-coated nanoparticle dispersions (after coating, rinsed with ultrapure water by centrifugation at 12,000g for 20 min, and resuspended in ultrapure water) with a Labconco Freezone 2.5 Plus freeze dryer. The samples were analyzed after a 5 min equilibration at 30 °C, and then the temperature was increased by a 5 °C/min ramp up to 1000 °C.

Antioxidant Properties. The nanoparticle antioxidant property was quantified by a colorimetric assay based on Cu²⁺ reduction (Sigma MAK187) and compared to that one of other antioxidant compounds: a 20 mg/mL commercial NC (Sigma 544841) dispersion in water, a 1 mg/mL curcumin (Sigma C1386), and a 10 mg/mL resveratrol (Sigma R5010) solution in ethanol. The assay enables quantification of antioxidant capacity of a substance in terms of Trolox (vitamin E analogue) equivalents. A Cu2+ working solution was added to nanoparticle dispersions, to other antioxidant compounds, and to serial dilutions of Trolox at known concentrations (for obtainment of a calibration curve, presented as Figure S2). In the presence of antioxidants, Cu2+ ions are reduced to Cu+ ions, which react with a colorimetric probe with an absorbance peak at 570 nm. All samples were incubated for 1 h, centrifuged at 16,000g for 20 min, and supernatant absorbance was measured with a VictorX3 microplate reader (PerkinElmer). All data are referred to 1 mg of antioxidant.

Dynamic Light Scattering and Z-Potential Measurements. Colloidal stability of nanoparticles dispersed in different aqueous media was investigated at different times of exposure (0, 2, 4, 6, 8, 10,

and 12 days) to 1g or s- μg (obtained by rotation in a random speed mode at 25–60°/s on a RPM, Airbus 2.0, equipped with a laptop and proprietary software for gravity level monitoring) at 37 °C. In particular, 100 μg /mL NC dispersions (both uncoated and FBS-coated) underwent colloidal stability studies in plain water, in 10% FBS (in water), and in complete proliferative medium with composition described in the following paragraph. For each dispersion, measurements were conducted in triplicate by three independent runs at 37 °C, and data are presented as average \pm standard deviation.

Biological Experiments. *Cell Cultures.* Human skeletal myoblasts (HSkM, Life Technologies A11440, at passage 3-5) were seeded at a density of $10,000 \text{ cells/cm}^2$ on Thermanox substrates $(1.05 \times 2.20 \text{ cm}^2)$, positioned at the bottom of homemade silicone holders), and they were allowed to adhere for 48 h prior to nanoparticle administration.

Biocompatibility Study. FBS-coated nanoparticles were administered at increasing concentrations (0, 10, 50, 100, 200, and 500 μg/mL) by dispersion in low-glucose Dulbecco's modified Eagle's medium (DMEM), added with 10% FBS, 25 mM HEPES, 2 mM L-glutamine, 100 U/mL penicillin, and 100 μg/mL streptomycin. Cultures were incubated for 24 and 96 h, then proliferation was assessed by Quant-iT PicoGreen assay. For this purpose, cell cultures were rinsed twice with PBS without $\text{Ca}^{2+}/\text{Mg}^{2+}$ and lysed by incubation with 500 μL of ultrapure water and three freeze/thaw cycles; ds-DNA was finally stained as recommended by the assay manufacturer. Fluorescence from ds-DNA was read by a microplate reader (excitation at 480 nm and emission at 520 nm). For each condition, measurements were conducted in triplicate by three independent runs at 37 °C, and data were presented as average \pm standard deviation.

Cell Culture under Simulated Microgravity. HSkM were seeded at a density of 3000 cells/cm² and allowed to adhere for 48 h prior to nanoparticle administration (final concentrations: 0 and 100 μ g/mL, also in the following analyses) and exposure to s- μ g. Myoblasts were seeded on Thermanox and on CaF² slides (for imaging/mapping purposes) or on polystyrene substrates (3 cm diameter Petri dishes, for other investigations). Cell cultures on Thermanox substrates (1.05 \times 2.20 cm²) were incubated with a volume of 1.4 mL of cell culture medium. With increasing cell culture surface of polystyrene substrates, volume was scaled up accordingly. Air bubble removal and liquid spill prevention were ensured by cell culture sealing with sterile Parafilm before loading on the RPM.

Nanoparticle Internalization Quantification: ICP-MS. For nanoparticle internalization studies, cell pellets were obtained by trypsinization and two sequential centrifugation runs at 700g for 10 min. After the first centrifugation, cell pellets were resuspended in PBS without ${\rm Ca^{2^+}/Mg^{2^+}}$ to ensure removal of free, not-internalized NC prior to the second centrifugation run. ICP-MS was conducted on cultures exposed to simulated microgravity upon dissolution in ${\rm H_2O_2/HNO_3}$ (2:1 v/v ratio) and sonication at 65 °C for 2 h. Lysate (200 $\mu{\rm L}$) was diluted in 10 mL of ultrapure water, and measurements were performed with a triple quadrupole spectrometer operating with the following parameters: 1550 W, 1 L/min nebulizer gas flow, 0.8 L/min auxiliary gas flow, 14 L/min coolant gas flow, 1.94 pyrane, 31 rpm pump speed, 32 °C interface temperature, and 2.7 °C chamber temperature.

Nanoparticle Internalization Quantification: Confocal Microscopy and Image Analysis. Cultures were fixed with 4% formaldehyde solution in PBS with Ca²⁺/Mg²⁺ for 20 min at 4 °C. Then, cells were permeabilized with a 0.1% Triton X-100 solution in PBS for 20 min. Saturation of aspecific antigenic sites was conducted with a 10% goat serum (GS) solution in PBS for 30 min, then an incubation with a 1:200 v/v dilution of primary antibodies (rabbit anti-caveolin, Abcam 2910, or mouse anti-clathrin, Abcam 2731) in 10% GS followed for 2 h at 37 °C. Samples were then rinsed three times with 10% GS (5 min each rinse) and thereafter incubated with a solution containing a 1:500 v/v dilution of secondary antibodies (TRITC-goat anti-rabbit, Invitrogen 2769 or TRITC-goat anti-mouse, Life Technologies A16071), 1:100 v/v dilution of Oregon Green 488-phalloidin (Life

Technologies 07466), and 1:100~v/v Hoechst dye (Life Technologies H21486) for 1 h at room temperature. Finally, samples were rinsed twice with PBS and imaged with a Nikon Ti-E confocal microscope. Ten images of optical fields were collected for each sample, and semi-automated image analysis for the measurement of Pearson's correlation coefficient (PCC) on light signal from proteins and NC was conducted with ImageJ software in order to elucidate possible nanoparticle internalization modalities.

Nanoparticle Internalization Analysis: TEM. For TEM imaging, samples were fixed in a 2.5% glutaraldehyde solution in 0.1 M sodium cacodylate buffer at 4 °C overnight. Samples were then washed three times for 10 min in the same buffer, and post-fixed in a solution of 1% osmium tetroxide/1% potassium ferrocyanide in 0.1 M sodium cacodylate for 1 h at 4 °C in the dark. After rinsing with buffer, specimens were incubated with a 0.15% tannic acid aqueous solution for 3 min, and they were again rinsed in chilled distilled water before dehydration (with 30, 50, 70, and 90% ethanol in water, performed on ice for 10 min, and eventually with 100% ethanol at room temperature). Then, samples were embedded in 1:1 epoxy resin/ ethanol mixture, and embedding was conducted in fresh Spuur's resin for 2 days before polymerization at 70 °C. Each sample was cut with a diamond knife in an ultramicrotome (FC7-UC5, Leica). Slices of 80 nm thickness were collected on a 200 mesh thin bar copper grid and stained with 1% uranyl acetate for 12 min in the dark. Imaging was performed by using a Tecnai G2 transmission electron microscope (ThermoFisher) equipped with a Veleta side-view camera, at 120 kV.

Nanoparticle Internalization Analysis: Raman Spectroscopy. Raman spectrum was collected as described in the Nanoparticle Characterization section on cultures grown on CaF_2 substrates, exposed to different gravity levels (1g and s- μg), and finally fixed with 4% formaldehyde solution in PBS. Raman spectrum was obtained by averaging 10 point-spectra for each experimental condition. Acquisition was done with a $100\times$ immersion objective. The obtained data were analyzed with the Raman Tool Set software (free available at https://sourceforge.net/projects/ramantoolset/). ¹³

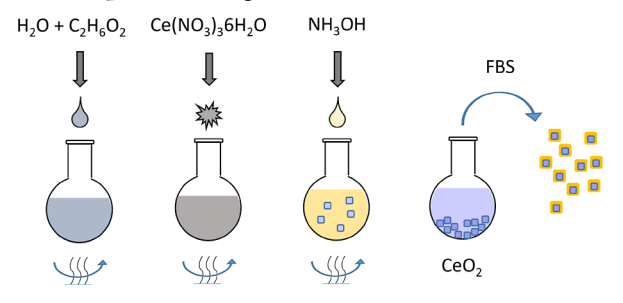
Quantitative Reverse Transcription-Polymerase Chain Reaction. Transcriptional effects of both nanoparticle administration and of s- μg exposure were studied by quantitative reverse transcription-polymerase chain reaction (qRT-PCR). After treatment, cell pellets were obtained by trypsinization and centrifugation at 700g for 10 min. Pellets were immediately stabilized with RNA fixative (RNAlater, Ambion) and freezing at $-80\,^{\circ}\text{C}$. RNA extraction and purification was conducted by removal of the fixative and cell lysis with phenol/ chloroform. After centrifugation at 12,000g for 15 min at 4 °C, the collected aqueous phase was incubated with equal volume of 70% ethanol, and then processed with the RNEasy Micro-RNA extraction/ purification kit (Qiagen), including a DNA digestion with DNAse on column, by following the manufacturer's instruction. Total RNA was eluted with 22 μ L of ultrapure water. Then, RNA yield and quality was assessed photometrically (NanoDrop), and a quantity of 200 ng of total RNA was reverse-transcribed with iScriptTM supermix (Bio-Rad), by applying the following thermal protocol: 5 min at 25 °C, 30 min at 42 °C, and 5 min at 85 °C with a CFX Connect thermal cycler (Bio-Rad). Polymerase chain reaction was conducted by mixing, for each well, 5 ng of cDNA (5 μ L) with SSO Advanced supermix (Bio-Rad, 10 μ L) and primers (500 nM final concentration, 5 μ L) and by applying the following thermal protocol (40 cycles): 5 s at 95 °C and 30 s at 60 °C. Primer sequences (obtained by Primer-BLAST software tool) are reported in Table S4. Data are presented as mean ± standard error of the mean.

Statistical Analysis. Statistical analysis was conducted by using the R software (https://www.r-project.org/). Two-tailed Student's t-test was used as a two-sample parametric test. For multiple comparisons, analysis of variance (ANOVA) parametric test was carried out, and, in the case of p < 0.05, Tukey's honestly significant difference post-hoc test was performed. Analysis of quantitative RT-PCR results was conducted with Bio-Rad CFX Manager software, and two-fold regulation was considered as a threshold. Significance was set at 0.001.

RESULTS AND DISCUSSION

Nanoparticle Characterization. Nanoparticle Synthesis. Nanoparticle synthesis was accomplished by simple ethylene glycol-assisted direct precipitation process, recapitulated in Scheme 1, yielding a precipitate that was successfully isolated by five cycles of centrifugation/resuspension in plain water to remove unreacted reagents and neutralize pH.

Scheme 1. Synthesis Process of Cerium Oxide Nanoparticles and Subsequent Coating with FBS



TEM Imaging. At the end of the synthetic/purification process, nanoparticles with a size of 8 ± 2 nm were obtained, as shown in Figure 1a, reporting a representative TEM image

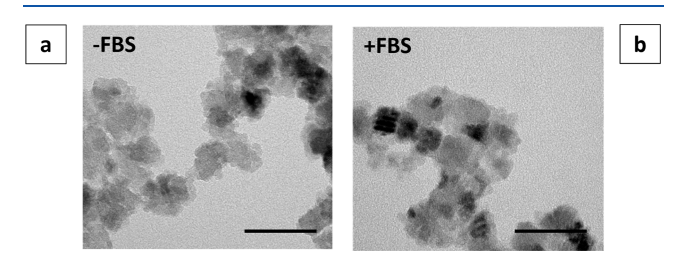


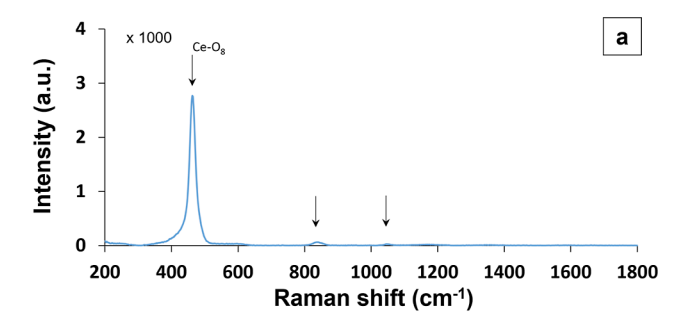
Figure 1. Representative TEM image of NC before (a) and after (b) coating with FBS. Scale bar is 25 nm.

of uncoated nanoparticles. Characterized by an irregular shape (in close agreement with the literature on similar synthetic processes ^{14,15}), these nanoparticles could easily be coated with FBS that did not alter original nanoparticle morphology, as shown in Figure 1b. Retention of the original NC morphology upon incubation with diluted protein coatings has previously been documented in the literature. ^{16,17}

Raman Spectroscopy. Reported in Figure 2a, Raman spectrum demonstrated the obtainment of cerium oxide by the characteristic first-order F_{2g} peak at 464 cm⁻¹ from symmetric stretching of the $Ce-O_8^{18}$ and by second-order peaks at 840 and 1050 cm⁻¹, in agreement with the literature. ^{18,19}

XPS Analysis. The expected chemical composition was confirmed by XPS. The survey spectrum reported in Figure 2b shows a Ce 3d peak (18.06%) at 883 eV and an O 1s peak (62.87%) at 530 eV, with minor peaks ascribable to unreacted reagents, that is a N 1s peak (7.22%) at 407 eV and a C 1s peak (11.86%) at 285 eV. The narrow spectrum of Ce 3d reported in Figure 2c enabled the quantification of the two oxidation states relevant to the exertion of antioxidant activity in vitro: Ce³⁺ (14.98%) and Ce⁴⁺ (85.02%), with the latter suggesting catalase-like antioxidant activity in the obtained nanoparticles.

XRD Analysis. XRD again confirmed the obtainment of NC, with a single cubic phase and an Fm-3m (225) fluorite



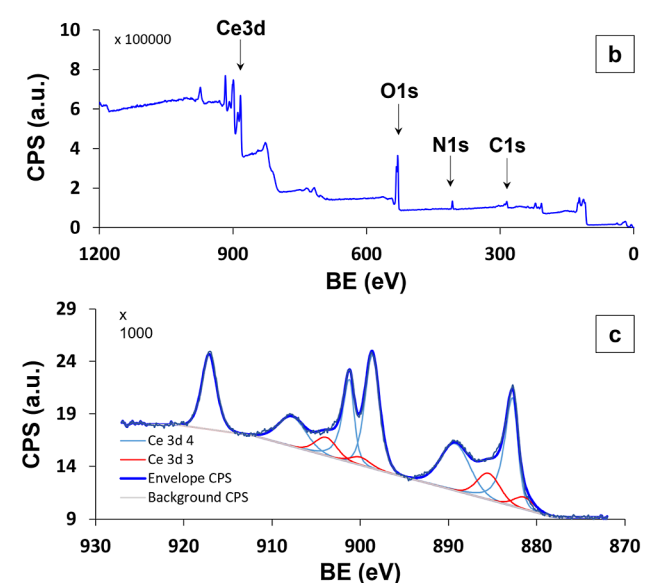


Figure 2. Representative Raman spectrum of the uncoated NC (a). XPS analysis, representative survey spectrum (b) and narrow spectrum (c) of uncoated NC.

structure, as shown in Figure S1a, and in agreement with the literature. ^{15,18} Table S1 reports XRD data concerning the crystallite size (in line with TEM imaging) and strain.

Thermal Gravimetric Analysis. As shown in Figure S1b, TGA demonstrated that the uncoated nanoparticles underwent a modest weight loss (12%) when the temperature was increased up to ~1000 °C, whereas the FBS-coated nanoparticles underwent a significant weight loss (~32%), denoting a conspicuous adsorption of serum that positively affects nanoparticle dispersion colloidal stability (see also dynamiclight scattering study reported later). Table S2 provides further details on the observed weight losses.

Antioxidant Property Analysis. Nanoparticle antioxidant property was quantified upon proper dilution of the stock dispersion through a colorimetric assay based on the reduction of Cu²⁺ ions, and it was compared to that one of the selected soluble antioxidant compounds. The assay calibration curve based on dilutions of a vitamin E analogue (Trolox) is reported in Figure S2. As shown in Table S3 (where all data refer to 1 mg of antioxidant), nanoparticles had a higher antioxidant property (235 nmol, expressed in Trolox equivalents) than other soluble antioxidants.

DLS and Zeta-Potential Measurement Analysis. A complete study on nanoparticle colloidal stability was conducted by comparison of dispersions kept at normal gravity and under s- μ g by rotation at 25–60°/s for a period of 12 days (Figure 3). In this study, the FBS coating stabilized the hydrodynamic diameter (HD) of nanoparticle dispersions in

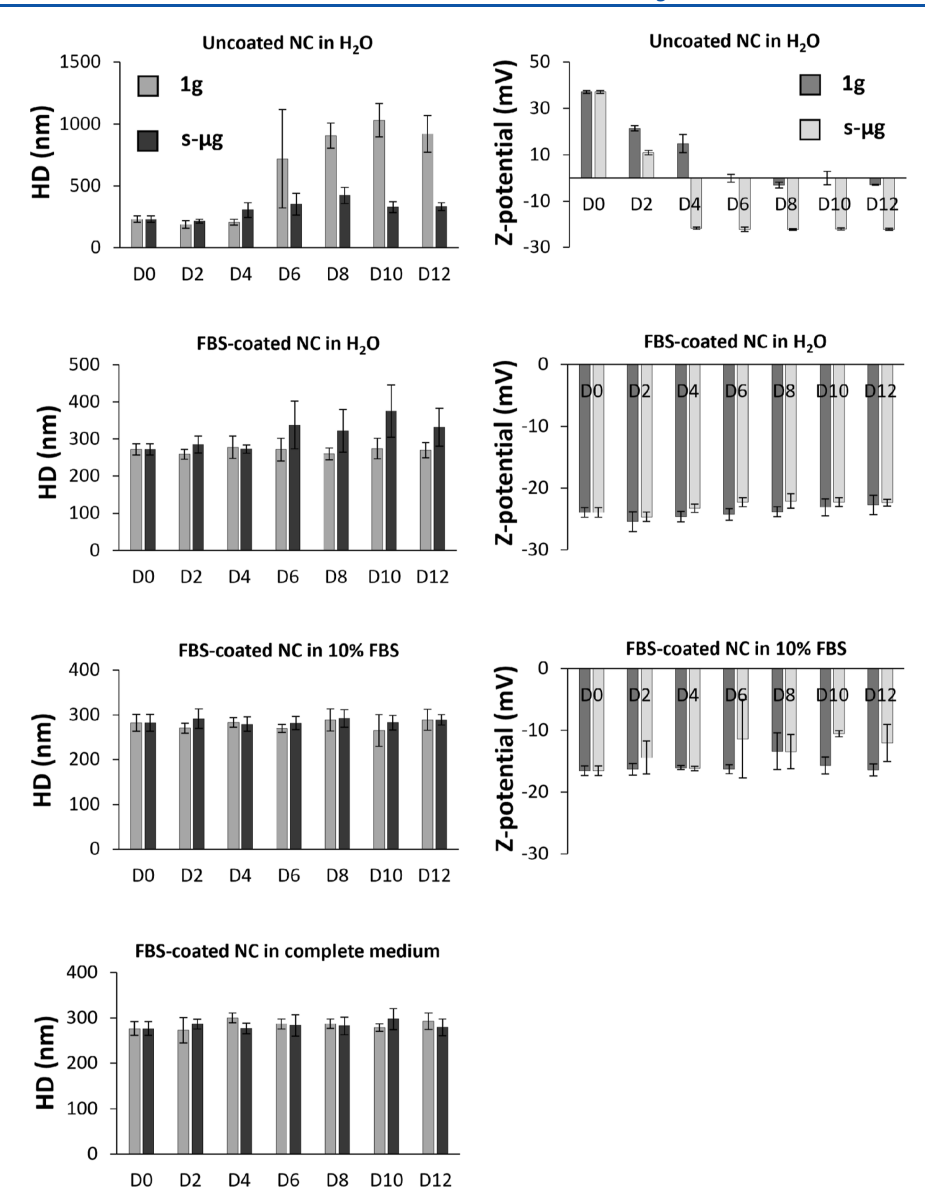


Figure 3. Time-course of colloidal stability measurements for $100 \mu g/mL$ NC dispersions (FBS-coated or uncoated) exposed to 1g or to $s-\mu g$ by $25-60^{\circ}/s$ rotation. HD stands for "hydrodynamic diameter" and D for "days".

the considered media (water, 10% FBS in water, and complete medium added with 10% FBS) compared to uncoated nanoparticle dispersions in water, to the point that no significant differences in HD could be found upon exposure to 1g or to s- μg for the whole observation period. A change in the Z-potential of uncoated nanoparticle dispersions in water over time was found, irrespective of gravity level. Further, the FBS coating determined the acquisition of a stable negative Zpotential for nanoparticle dispersions in the considered media, again independently on gravity level. These findings are in line with what is reported in the literature concerning transition of Z-potential of uncoated NC in water from positive to negative, ascribable to solvation ion and counterion turnover at the nanoparticle surface.²² Interest in the interaction of carefully selected nanoparticle dispersions with biological models under real and simulated microgravity has recently emerged in the scientific community for the potential to address noxious effects of gravitational unloading and cosmic radiation exposure during spaceflight. Assessment of long-term colloidal properties of nanoparticle dispersions for biomedical purposes

is in particular a complete novelty in the field of altered gravity science and represents a crucial topic to be investigated in view of possible nanomaterial storage and following administration during spaceflight. The literature review revealed scant studies on the colloidal properties of nanoparticle dispersions under s- μg conditions. Among these, there is a long-term study (14 days) performed by our group on commercial NC with a heterogeneous size (motivating nanoparticle synthesis in this work), in line with the present colloidal stability data on synthesized NC with a monodisperse size. 11 Another recent study assessed colloid dynamics of a dispersion of ~8 nm gold nanoparticles featuring an oleylamine shell in an organic solvent on a drop tower.²³ This study demonstrated the retention of nanoparticle dispersion HD (~21 nm) and diffusivity in a fast temperature gradient, but only concerning the short time period of s-µg accessible on drop tower, that is of 9.1 s. Among the studies on nanoparticle dispersions in biocompatible solvents, there is the abovementioned one concerning polylactic acid and polyhydroxyalkanoate nanoparticles for drug delivery to adipose-derived stem cells under

s- μg , showing the assessment of nanoparticle HD (90–200 nm) and Z-potential (\sim -7 mV) only at one time point. Another study also assessed colloidal stability of titanium dioxide nanoparticle dispersions with potential cytotoxic effects on pulmonary epithelial cells under s- μg at a single time point (HD \sim 120 nm and Z-potential \sim -22 mV).²⁴ Both studies implied short-term interaction between nanoparticle dispersions and their cellular targets (<48 h). To the best of our knowledge, only one study investigated colloidal stability of different drug nanoemulsions (carbamazepine, fenofibrate, melatonin) under s-µg for 7 days. This investigation demonstrated modest fluctuations in both HD and Z-potential over time and suggested suitability of these formulations to longer term studies under simulated microgravity.²⁵ Overall, our studies provide unprecedented and unique indications on long-term nanoparticle dispersion stability under altered gravity conditions.

Biological Experiments. *Biocompatibility Study.* As shown in Figure S3, HSkM exhibited comparable viability in the presence of all NC concentrations tested at 24 h from nanoparticle administration. The cell population underwent regular proliferation up to 200 μ g/mL NC.

Nanoparticle Internalization Quantification: ICP-MS Analysis. Internalization of FBS-coated NC by HSkM exposed to s- μg (by 25–60°/s rotation) was then investigated by ICP-MS, and its occurrence was verified, although at a lower extent compared to 1g. As shown in Figure 4, NC internalization after

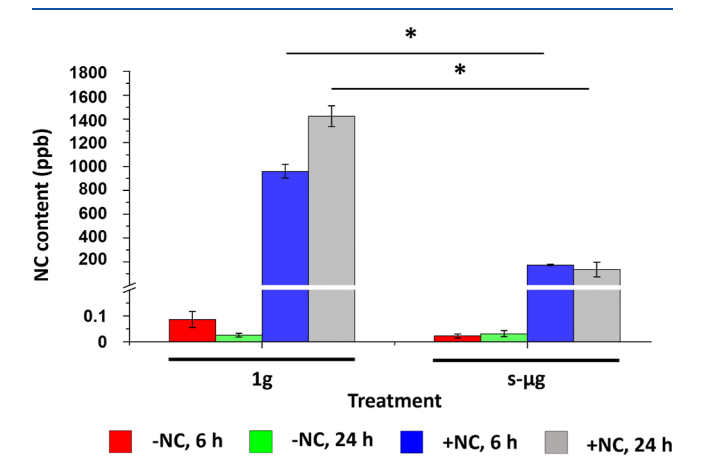


Figure 4. ICP-MS analysis of NC internalization by HSkM cultures exposed to 1g or s- μ g for 6 and 24 h. (*p < 0.001).

6 and 24 h of s- μ g was \sim 6x and \sim 11x lower than that found at 1g, respectively. Under s- μ g, nanoparticle internalization did not increase over time, unlike at 1g. Nanoparticle concentration at 24 h was indeed \sim 50% higher than at 6 h. Increment of nanoparticle internalization over time under normal gravity can be explained by considering that diluted colloids at a steady state show an inhomogeneous nanoparticle distribution along the gravity direction, corresponding to an exponential concentration distribution. When colloids are administered to cell cultures under normal gravity, there is an increasing availability of nanoparticles in proximity of the cells over time, hence the increasing internalization.

Nanoparticle Internalization Study: Confocal Microscopy and Image Analysis. Analysis of NC internalization by HSkM after 6 and 24 h of culture was conducted by confocal microscopy. For this purpose, immunofluorescence staining of

caveolin-1 and clathrin was performed in cell cultures exposed to $25-60^{\circ}/s$ rotation and in those kept at 1g. As depicted in Figures S4 and S5, all cultures were characterized by intracellular spots compatible to light scattering from large NC aggregates (shown in pink, upon irradiation with laser light of $\lambda = 647$ nm). NC signal did not apparently co-localize with fluorescence from immunostaining of caveolin-1 or clathrin (shown in green) at both gravity levels. This was confirmed through PCC measurements by image analysis for both markers in the different experimental classes (Figure S6), thus excluding internalization of NC aggregates by caveolin-1 or clathrin at the selected observation time points.

Nanoparticle Internalization Analysis: TEM. NC internalization by HSkM after 6 and 24 h of culture was also studied by TEM. Figure 5 shows that cells incubated with nano-

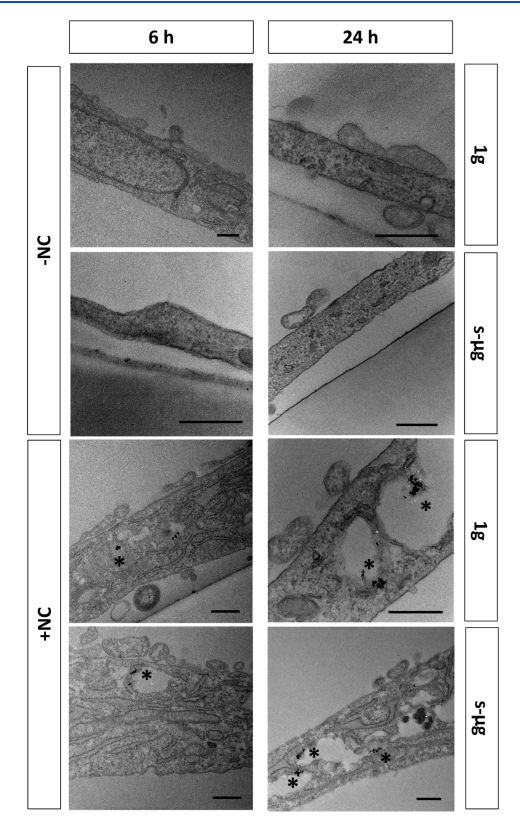


Figure 5. Representative TEM images of HSkM either treated or not with FBS-coated NC and exposed to 1g or to s-µg for 6 and 24 h. Scale bar is 500 nm. Asterisks evidence intracellular NC location.

particles well retained their ultrastructure, suggesting that NC had no cytotoxic effects in the chosen observation timeframe. NC-treated cells were characterized by intracellular electrondense spots ascribable to small NC aggregates at both gravity levels: these spots were obviously lacking in untreated cells and again demonstrate that NC were internalized despite the gravitational unloading applied at nanoparticle administration. At 6 h from administration, nanoparticle aggregates localized in the cytosol and mostly at the periphery of large endocytic compartments, whereas they became larger and retained their positioning at the edges of endocytic compartments at 24 h from administration, irrespective of gravity levels. Nanoparticles were not found in the mitochondria and nuclei. Presence of extensive membrane ruffling in specimens at both gravity levels suggests that nanoparticle internalization by

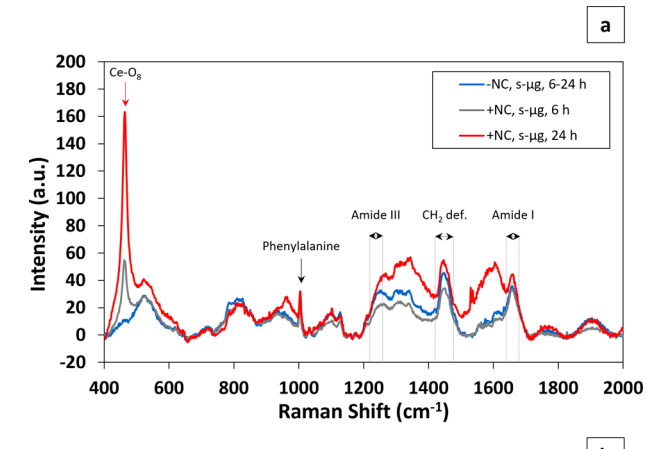
HSkM mainly occurred through macropinocytosis, coherently with the observation of nanoparticle aggregates associated to several endocytic compartments with size exceeding 500 nm²⁷ and of membrane invaginations devoid of nanoparticles (Figure S7).

Like NC colloidal stability investigations, the microscopy analysis results offered an unprecedented insight on early nanomaterial interactions with cell culture models under altered gravity conditions. TEM data on nanoparticleadministered cultures showing uptake mainly through macropinocytosis contribute to the variety of reports on NC internalization modes described in the literature. Demonstrated to undergo macropinocytosis also in mammary adenocarcinoma cells, 28 NC were, for instance, additionally shown to undergo caveolin-1 and clathrin-mediated endocytosis by endothelial cells,²⁹ adenocarcinoma alveolar basal epithelial cells,³⁰ and keratinocytes.³¹ Altogether, these pieces of evidence reinforce the notion that NC internalization depends on factors intrinsic to nanoparticle features, like size and charge,³¹ along with extrinsic ones, like protein corona composition, surface coating, and cell target. 30,32,33 The present nanoparticle association to endocytic compartments is in line with other reports in the literature 29,30,34 and underlies possible exertion of antioxidant catalase-like activity, as identified by administration of Ce4+-rich NC to human hepatic cells²¹ and by abundance of Ce⁴⁺ from NC localized in endocytic compartments of cervical carcinoma epithelial cells.33

Nanoparticle Internalization Analysis: Raman Spectroscopy. NC internalization by HSkM after 6 and 24 h of culture was also studied by Raman spectroscopy (Figure 6). Similar to Figures 2a and 6a,b (related to cultures kept at 1g and s- μ g cultures, respectively) shows the characteristic first-order F_{2g} peak at 464 cm⁻¹ from symmetric stretching of Ce-O₈ for all spectra of NC-treated cultures. Nanoparticle internalization in NC-treated cultures was confirmed by co-detection of signals corresponding to biomacromolecules, such as phenylalanine (at 1003 cm⁻¹), nucleic acids (at 1095 cm⁻¹ for DNA backbone, O-P-O stretching), and proteins and lipids (at $1220-1260 \text{ cm}^{-1}$ for Amide-III, at $1420-1490 \text{ cm}^{-1}$ for $C-H_2$ deformation, and 1660-1690 cm⁻¹ for Amide I, C-C). 36,37 In agreement with ICP-MS data collected from cultures kept at 1g, NC internalization increased with incubation time, as arguable from increasing F_{2g} peak intensity (evidenced by the red arrow in Figure 6a).

Transcriptional Analysis. As shown in Figure 7 and detailed in Table 1, cultures exposed to s- μg for 6 h underwent ~3-fold upregulation of Nos1 compared to cultures kept at 1g. Cultures exposed to s-µg for 24 h underwent 2-fold downregulation of Sod2 compared to cultures kept at normal gravity. NC-treated cultures underwent upregulation of Sod2 compared to untreated cultures at both time points, irrespective of gravity levels. NC-treated cultures indeed underwent 2-fold and 20fold upregulation of Sod2 compared to untreated cultures, respectively, after 6 and 24 h at 1g. They underwent ~2-fold and ~16-fold upregulation of Sod2 compared to untreated cultures, respectively after 6 and 24 h under s-µg. NC-treated cultures demonstrated ~2-fold upregulation of Sod3 at the transcriptional level after 6 h of treatment under s- μg and ~ 3 fold upregulation after 24 h of treatment under both gravity levels.

Transcriptional data suggest important regulatory effects of nanoparticle administration to cultures. In skeletal muscle,



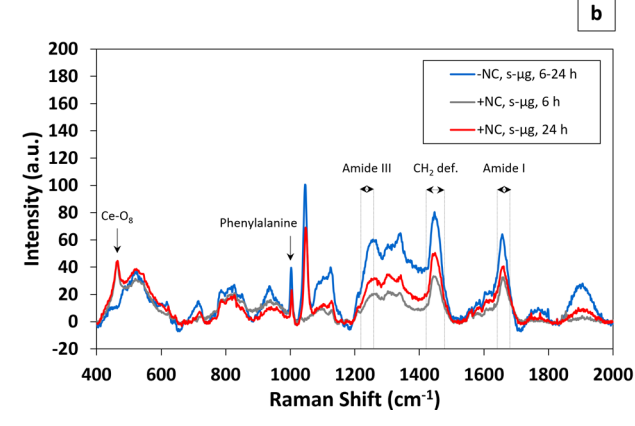


Figure 6. Raman analysis of NC internalization by HSkM cultures exposed to 1g (a) or s- μg (b). "Def." stands for "deformation".

nitric oxide synthase is the main source of NO, an important signaling molecule accomplishing dual functions of muscle mass maintenance/growth and breakdown, depending on complex regulatory mechanisms, also on a redox base.³⁸ Since long-term spaceflight is known to affect NOS1 expression at the soleus muscle level in mice by decreasing the sarcolemmal-to-cytoplasmic protein ratio (thus implying NOS1 dislocation), tools for regulation of this enzyme expression are recognized as crucial in counteracting microgravity-induced muscle wasting.³⁹ In this work, both simulated microgravity and nanoparticle administration were found to have regulatory effects on Nos1 transcription. The prominent Nos1 upregulation observed in HSkM cultures at 24 h following nanoparticle administration under both gravity levels appears well coherent with evidence in the literature on NO scavenging activity by NC characterized by high Ce4+ percentage. 40 It also suggests the opportunity of performing analyses at the translational level and at later time points, aiming at assessing possible effects on myoblast function.

Interestingly, Sod2 underwent upregulation in NC-treated cultures under s- μg for 6 h compared to those kept at 1g, whereas it underwent downregulation at 24 h. A similar transcriptional pattern was observed also for Sod3: altogether, these data suggest complex interplay of treatments in affecting transcription of crucial markers involved in antioxidant response. Superoxide dismutase 2 is a member of the iron/manganese superoxide dismutase family. Sod2 gene encodes for a protein of the mitochondrial matrix catalyzing superoxide radical conversion into hydrogen peroxide and molecular oxygen and preventing superoxide-mediated generation of

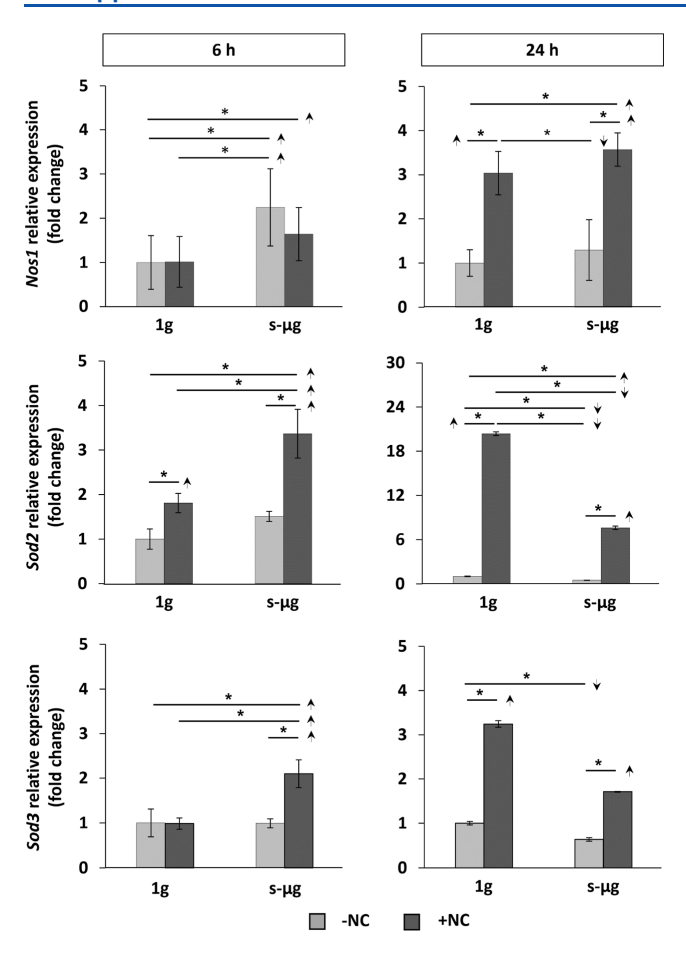


Figure 7. qRT-PCR analysis of marker genes involved in antioxidant response, relative expression levels of *Nos1*, *Sod2*, and *Sod3* normalized to *Rpl32*, as a reference gene (*p < 0.001, 2-fold regulation threshold).

Table 1. Marker Gene Regulation^a

	marker	marker gene (after 6 h)			marker gene (after 24 h)		
comparison $(p < 0.001)$	Nos1	Sod2	Sod3	Nos1	Sod2	Sod3	
(+NC, s-µg) vs (-NC, 1g)	2.34	4.8	2.99	3.57	7.62	-	
(-NC, s-μg) vs (-NC, 1g)	2.97	-	-	-	-2.08	-	
(+NC, 1g) vs (-NC, 1g)	-	2.11	-	3.04	20.38	3.24	
(+NC, s-μg) vs (+NC, 1g)	-	2.27	2.61	-	-2.67	-	
(-NC, s-μg) vs (+NC, 1g)	2.52	-	_	-2.34	-42.46	-5.1	
(+NC, s-\mu g) vs (-NC, s-\mu g)	-	2.4	2.29	2.75	15.87	2.69	

a"-": significant regulation exceeding value of 2 not available.

more reactive species, like hydroxyl radicals and peroxynitrite. *Sod2* is known to play a crucial role in intracellular redox state balance, and its regulation has important implications both *in vitro* and *in vivo*. Overexpression of *Sod2* in mouse myoblasts was indeed shown to have protective effects on mitochondrial DNA abundance and on some mitochondrial functions (for instance, succinate dehydrogenase activity), as well as preserving myoblast differentiation potential *in vitro*. ⁴¹ Interestingly, *Sod2* overexpression in a dose-dependent manner

was also found, along with decreased ROS production, in normal human colon cells administered with increasing concentrations of NC before exposure to single-dose 20 Gy radiation. Administration of the same nanoparticles to athymic nude mice resulted in a decrease of TUNEL- and caspase 3positive cells, as well as in an increase of Sod2 expression in gastrointestinal epithelium at 4 h from irradiation, suggesting important radioprotective effects of NC on these in vitro and in vivo models. 42 In this work, HSkM treated with nanoparticles underwent a significant Sod2 upregulation at both gravity levels and analysis time points with respect to untreated myoblasts. Notably, HSkM incubation with NC for 24 h under normal gravity determined a ~20-fold overexpression of Sod2 marker in comparison to untreated cultures. Along with the observation of Sod2 downregulation in NC-untreated cultures exposed to simulated microgravity for 24 h in comparison to static cultures, these data support the need for further investigations on NC potential in protecting mitochondrial function under altered gravity conditions. Mitochondrial dysregulation targeting in real and simulated microgravity has indeed been recognized by the scientific community as a crucial topic that could enable longer human permanence in space.4

Superoxide dismutase 3 is a member of the copper/zinc superoxide dismutase family. Sod3 gene encodes for a protein accomplishing antioxidant activity on the extracellular environment. Overexpression of Sod3 in human skeletal musclederived stem/progenitor cells (HSkMDS/PCs) after lentiviralmediated transduction was found to prevent cell ageing and apoptosis under normoxia and hypoxia cell culture conditions. Sod3 overexpression was also associated to a higher myoblast fusion into myotubes under both normoxia and hypoxia conditions. Interestingly, HSkMDS/PCs overexpressing Sod3 after plasmid-mediated transfection demonstrated significantly higher transcriptional levels of Sod2 (40-fold upregulation) under both normoxia and hypoxia conditions. Transfected cells also showed higher transcriptional levels of antiaging marker Foxo (~3-fold upregulation) under both oxygenation conditions and of antiapoptotic marker Bcl2 (~2-fold upregulation) under hypoxia, as well as regulation of differentiation markers MyoD (~18-fold upregulation) and Myog (2-fold downregulation) under normoxia.⁴⁴ In this work, Sod3 overexpression in NC-treated HSkM correlates with much higher Sod2 overexpression levels, thus encouraging investigations on the antioxidant response regulation and on the myogenic potential of NC administration.

CONCLUSIONS

This work presents the synthesis of nanoparticles with very high antioxidant activity, far exceeding that one of well-known soluble compounds, and their administration to a skeletal muscle model under simulated microgravity conditions. Internalization under simulated microgravity was verified to occur to a lower extent than under normal gravity. The collected data suggest HSkM preferential nanoparticle internalization through macropinocytosis under both normal and simulated microgravity, although to a lower extent in gravitational unloading conditions. Within 24 h from administration, nanoparticles accumulated in the cytosol and in large endocytic compartments, compatible with the observed preferential internalization modality. This work demonstrated that nanoparticles are internalized by cell cultures even when delivered concomitantly to the application

of microgravity simulation conditions. NC exerts strong biological effects ascribable to oxidative stress alleviation both on the intracellular and the extracellular environment, as arguable from transcriptional analyses showing strong regulation of key marker genes involved in antioxidant response. Regulation of antioxidant response apparently occurs within 24 h from nanoparticle administration, with possible effects expected also at later time points and deserving further investigations, in view of myogenesis potential assessment and myotube formation promotion and retention under simulated microgravity.

ASSOCIATED CONTENT

s Supporting Information

The Supporting Information is available free of charge at https://pubs.acs.org/doi/10.1021/acsanm.3c02230.

Nanoparticle characterization by XRD and TGA; XRD analysis results; TGA analysis results; calibration curve in antioxidant capacity quantification; *in vitro* antioxidant analysis results; NC cytotoxicity analysis results; caveolin-1 immunofluorescence; clathrin immunofluorescence; analysis of NC colocalization with either caveolin-1 and clathrin; TEM imaging of cell membrane invaginations; and oligonucleotide sequences for qRT-PCR (PDF)

AUTHOR INFORMATION

Corresponding Authors

Giada Graziana Genchi — Istituto Italiano di Tecnologia, Smart Bio-Interfaces, Pontedera 56025, Italy; Email: giada.genchi@iit.it

Gianni Ciofani — Istituto Italiano di Tecnologia, Smart Bio-Interfaces, Pontedera 56025, Italy; o orcid.org/0000-0003-1192-3647; Email: gianni.ciofani@iit.it

Authors

Valentina Mollo – Istituto Italiano di Tecnologia, Bio-Logic Materials, Napoli 80125, Italy

Matteo Battaglini — Istituto Italiano di Tecnologia, Smart Bio-Interfaces, Pontedera 56025, Italy

Melike Belenli Gümüş — Istituto İtaliano di Tecnologia, Smart Bio-Interfaces, Pontedera 56025, İtaly; Scuola Superiore Sant'Anna, The BioRobotics Institute, Pontedera 56025, İtaly

Attilio Marino — Istituto Italiano di Tecnologia, Smart Bio-Interfaces, Pontedera 56025, Italy; o orcid.org/0000-0002-3290-494X

Mirko Prato − Istituto Italiano di Tecnologia, Materials Characterization Facility, Genova 16163, Italy; orcid.org/0000-0002-2188-8059

Sergio Marras – Istituto Italiano di Tecnologia, Materials Characterization Facility, Genova 16163, Italy

Filippo Drago – Istituto Italiano di Tecnologia, Nanochemistry, Genova 16163, Italy

Giammarino Pugliese – Istituto Italiano di Tecnologia, Materials Characterization Facility, Genova 16163, Italy

Francesca Santoro – Istituto Italiano di Tecnologia, Bio-Logic Materials, Napoli 80125, Italy

Complete contact information is available at: https://pubs.acs.org/10.1021/acsanm.3c02230

Author Contributions

G.G.G. conceived and performed all experimental activities involving nanoparticle synthesis and testing with cell cultures. V.M. and F.S. performed electron microscopy on cell cultures. M.B. performed Raman spectroscopy, confocal microscopy, and image analysis. M.B.G. conducted Raman spectroscopy analysis on synthesized nanoparticles. A.M. performed Raman spectroscopy analysis and statistical analysis. M.P., S.M., F.D., and G.P. respectively collected XPS, XRD, ICP-MS, and TGA data. G.C. supervised all experimental activities. The manuscript was written through contributions of all authors. All authors have given approval to the final version of the manuscript.

Notes

The authors declare no competing financial interest. All data are available from authors upon reasonable request.

ACKNOWLEDGMENTS

The European Space Agency (ESA) is gratefully acknowledged for co-funding this research with contract 4000129652/20/NL/MH/ac (ESA-OSIP InterGravity project). Dr. François Gaubert (ESA) is kindly acknowledged for fruitful discussions during project implementation. Dr. Rosaria Brescia (IIT) is kindly acknowledged for TEM imaging on nanoparticles.

REFERENCES

- (1) Vernikos, J.; Schneider, V. S. Space, gravity and the physiology of aging: Parallel or convergent disciplines? A mini-review. *Gerontology* **2010**, *56*, 157–166.
- (2) Strollo, F.; Gentile, S.; Strollo, G.; Mambro, A.; Vernikos, J. Recent progress in space physiology and aging. *Front. Physiol.* **2018**, *9*, 1–9.
- (3) Clément, G. R.; Boyle, R. D.; George, K. A.; Nelson, G. A.; Reschke, M. F.; Williams, T. J.; Paloski, W. H. Challenges to the central nervous system during human spaceflight missions to Mars. *J. Neurophysiol.* **2020**, *123*, 2037–2063.
- (4) Genah, S.; Monici, M.; Morbidelli, L. The effect of space travel on bone metabolism: Considerations on today's major challenges and advances in pharmacology. *Int. J. Mol. Sci.* **2021**, 22, 4585.
- (5) Furukawa, S.; Chatani, M.; Higashitani, A.; Higashibata, A.; Kawano, F.; Nikawa, T.; Numaga-Tomita, T.; Ogura, T.; Sato, F.; Sehara-Fujisawa, A.; et al. Findings from recent studies by the Japan Aerospace Exploration Agency examining musculoskeletal atrophy in space and on Earth. *npj Microgravity* **2021**, *7*, 18.
- (6) Costa, F.; Ambesi-Impiombato, F. S.; Beccari, T.; Conte, C.; Cataldi, S.; Curcio, F.; Albi, E. Spaceflight Induced Disorders: Potential Nutritional Countermeasures. *Front. Bioeng. Biotechnol.* **2021**, *9*, 1–8.
- (7) English, K. L.; Downs, M.; Goetchius, E.; Buxton, R.; Ryder, J. W.; Ploutz-Snyder, R.; Guilliams, M.; Scott, J. M.; Ploutz-Snyder, L. L. High intensity training during spaceflight: results from the NASA Sprint Study. *npj Microgravity* **2020**, *6*, 21.
- (8) Cristofaro, F.; Pani, G.; Pascucci, B.; Mariani, A.; Balsamo, M.; Donati, A.; Mascetti, G.; Rea, G.; Rizzo, A. M.; Visai, L. The NATO project: nanoparticle-based countermeasures for microgravity-induced osteoporosis. *Sci. Rep.* **2019**, *9*, 17141–17215.
- (9) Zhao, X. H.; Peng, X. L.; Gong, H. L.; Wei, D. X. Osteogenic differentiation system based on biopolymer nanoparticles for stem cells in simulated microgravity. *Biomed. Mater.* **2021**, *16*, 044102.
- (10) Genchi, G. G.; Degl'Innocenti, A.; Salgarella, A. R.; Pezzini, I.; Marino, A.; Menciassi, A.; Piccirillo, S.; Balsamo, M.; Ciofani, G. Modulation of gene expression in rat muscle cells following treatment with nanoceria in different gravity regimes. *Nanomedicine* **2018**, *13*, 2821–2833.
- (11) Genchi, G. G.; Degl'Innocenti, A.; Martinelli, C.; Battaglini, M.; De Pasquale, D.; Prato, M.; Marras, S.; Pugliese, G.; Drago, F.;

- Mariani, A.; et al. Cerium Oxide Nanoparticle Administration to Skeletal Muscle Cells under Different Gravity and Radiation Conditions. ACS Appl. Mater. Interfaces 2021, 13, 40200–40213.
- (12) Arya, A.; Sethy, N. K.; Gangwar, A.; Bhargava, N.; Dubey, A.; Roy, M.; Srivastava, G.; Singh, S. K.; Das, M.; Bhargava, K. Cerium oxide nanozyme modulate the 'exercise' redox biology of skeletal muscle. *Mater. Res. Express* **2017**, *4*, 055401.
- (13) Candeloro, P.; Grande, E.; Raimondo, R.; Di Mascolo, D.; Gentile, F.; Coluccio, M. L.; Perozziello, G.; Malara, N.; Francardi, M.; Di Fabrizio, E. Raman database of amino acids solutions: a critical study of Extended Multiplicative Signal Correction. *Analyst* **2013**, *138*, 7331–7340.
- (14) Caputo, F.; Mameli, M.; Sienkiewicz, A.; Licoccia, S.; Stellacci, F.; Ghibelli, L.; Traversa, E. A novel synthetic approach of cerium oxide nanoparticles with improved biomedical activity. *Sci. Rep.* **2017**, 7, 4636–4714.
- (15) Natile, M. M.; Boccaletti, G.; Glisenti, A. Properties and reactivity of nanostructured CeO2 powders: Comparison among two synthesis procedures. *Chem. Mater.* **2005**, *17*, 6272–6286.
- (16) Shah, V.; Shah, S.; Shah, H.; Rispoli, F. J.; McDonnell, K. T.; Workeneh, S.; Karakoti, A.; Kumar, A.; Seal, S. Antibacterial Activity of Polymer Coated Cerium Oxide Nanoparticles. *PLoS One* **2012**, *7*, No. e47827.
- (17) Nawaz, M.; Shakoor, R. A.; Kahraman, R.; Montemor, M. F. Cerium oxide loaded with Gum Arabic as environmentally friendly anti-corrosion additive for protection of coated steel. *Mater. Des.* **2021**, *198*, 109361.
- (18) Jayakumar, G.; Albert Irudayaraj, A.; Dhayal Raj, A. A comprehensive investigation on the properties of nanostructured cerium oxide. *Opt. Quantum Electron.* **2019**, *51*, 312–315.
- (19) Zamiri, R.; Abbastabar Ahangar, H.; Kaushal, A.; Zakaria, A.; Zamiri, G.; Tobaldi, D.; Ferreira, J. M. F. Dielectrical properties of CeO2 nanoparticles at different temperatures. *PLoS One* **2015**, *10*, No. e0122989.
- (20) Pirmohamed, T.; Dowding, J. M.; Singh, S.; Wasserman, B.; Heckert, E.; Karakoti, A. S.; King, J. E. S.; Seal, S.; Self, W. T. Nanoceria exhibit redox state-dependent catalase mimetic activity. *Chem. Commun.* **2010**, *46*, 2736–2738.
- (21) Singh, R.; Singh, S. Redox-dependent catalase mimetic cerium oxide-based nanozyme protect human hepatic cells from 3-AT induced acatalasemia. *Colloids Surf. B Biointerfaces* **2019**, *175*, 625–635
- (22) Vincent, A.; Inerbaev, T. M.; Babu, S.; Karakoti, A. S.; Self, W. T.; Masunov, A. E.; Seal, S. Tuning hydrated nanoceria surfaces: Experimental/theoretical investigations of ion exchange and implications in organic and inorganic interactions. *Langmuir* **2010**, *26*, 7188–7198.
- (23) Pyttlik, A.; Kuttich, B.; Kraus, T. Dynamic Light Scattering on Nanoparticles in Microgravity in a Drop Tower. *Microgravity Sci. Technol.* **2022**, *34*, 13.
- (24) Wang, M.; Li, J.; Zhang, S.; You, Y.; Zhu, X.; Xiang, H.; Yan, L.; Zhao, F.; Li, Y. Effects of Titanium Dioxide Nanoparticles on Cell Growth and Migration of A549 Cells under Simulated Microgravity. *Nanomaterials* **2022**, *12*, 1879–1921.
- (25) Dantuma, D.; et al. Impact of Simulated Microgravity on Nanoemulsion Stability A Preliminary Research. *Am. J. Med. Biol. Res.* **2015**, *3*, 102–106.
- (26) Vailati, A.; Bataller, H.; Bou-Ali, M. M.; Carpineti, M.; Cerbino, R.; Croccolo, F.; Egelhaaf, S. U.; Giavazzi, F.; Giraudet, C.; Guevara-Carrion, G.; et al. Diffusion in liquid mixtures. *npj Microgravity* **2023**, *9*, 1–8.
- (27) Jin, J.; Shen, Y.; Zhang, B.; Deng, R.; Huang, D.; Lu, T.; Sun, F.; Xu, S.; Liang, C. In situ exploration of characteristics of macropinocytosis and size range of internalized substances in cells by 3D-structured illumination microscopy. *Int. J. Nanomed.* **2018**, *13*, 5321–5333.
- (28) Bibb, E.; Alajlan, N.; Alsuwailem, S.; Mitchell, B.; Brady, A.; Maqbool, M.; George, R. Internalized Nanoceria Modify the

- Radiation-Sensitivity Profile of MDA MB231 Breast Carcinoma Cells. *Biology* **2021**, *10*, 1148.
- (29) Chen, S.; Hou, Y.; Cheng, G.; Zhang, C.; Wang, S.; Zhang, J. Cerium oxide nanoparticles protect endothelial cells from apoptosis induced by oxidative stress. *Biol. Trace Elem. Res.* **2013**, *154*, 156–166.
- (30) Mazzolini, J.; Weber, R. J. M.; Chen, H. S.; Khan, A.; Guggenheim, E.; Shaw, R. K.; Chipman, J. K.; Viant, M. R.; Rappoport, J. Z. Protein corona modulates uptake and toxicity of nanoceria via clathrin-mediated endocytosis. *Biol. Bull.* **2016**, 231, 40–60.
- (31) Singh, S.; Kumar, A.; Karakoti, A.; Seal, S.; Self, W. T. Unveiling the mechanism of uptake and sub-cellular distribution of cerium oxide nanoparticles. *Mol. Biosyst.* **2010**, *6*, 1813–1820.
- (32) Asati, A.; Santra, S.; Kaittanis, C.; Perez, J. M. Surface-Charge-Dependent Cell Localization and Cytotoxicity of Cerium Oxide Nanoparticles. *ACS Nano* **2010**, *4*, 5321–5331.
- (33) Vassie, J. A.; Whitelock, J. M.; Lord, M. S. Endocytosis of cerium oxide nanoparticles and modulation of reactive oxygen species in human ovarian and colon cancer cells. *Acta Biomater.* **2017**, *50*, 127–141.
- (34) Del Turco, S.; Cappello, V.; Tapeinos, C.; Moscardini, A.; Sabatino, L.; Battaglini, M.; Melandro, F.; Torri, F.; Martinelli, C.; Babboni, S.; et al. Cerium oxide nanoparticles administration during machine perfusion of discarded human livers: A pilot study. *Liver Transplant.* **2022**, *28*, 1173–1185.
- (35) Ferraro, D.; Tredici, I. G.; Ghigna, P.; Castillio-Michel, H.; Falqui, A.; Di Benedetto, C.; Alberti, G.; Ricci, V.; Anselmi-Tamburini, U.; Sommi, P. Dependence of the Ce(III)/Ce(IV) ratio on intracellular localization in ceria nanoparticles internalized by human cells. *Nanoscale* **2017**, *9*, 1527–1538.
- (36) Fujita, K.; Smith, N. I. Label-Free Molecular Imaging of Living Cells. *Mol. Cells* **2008**, *26*, 530–535.
- (37) Su, L.; Chen, Y.; Zhang, G. N.; Wang, L. H.; Shen, A. G.; Zhou, X. D.; Wang, X. H.; Hu, J. M. In vivo and in situ monitoring of the nitric oxide stimulus response of single cancer cells by Raman spectroscopy. *Laser Phys. Lett.* **2013**, *10*, 045608.
- (38) Kobayashi, J.; Uchida, H.; Kofuji, A.; Ito, J.; Shimizu, M.; Kim, H.; Sekiguchi, Y.; Kushibe, S. Molecular regulation of skeletal muscle mass and the contribution of nitric oxide: A review. *FASEB BioAdvances* **2019**, *1*, 364–374.
- (39) Sandonà, D.; Desaphy, J. F.; Camerino, G. M.; Bianchini, E.; Ciciliot, S.; Danieli-Betto, D.; Dobrowolny, G.; Furlan, S.; Germinario, E.; Goto, K.; et al. Adaptation of mouse skeletal muscle to long-term microgravity in the MDS mission. *PLoS One* **2012**, *7*, No. e33232.
- (40) Dowding, J. M.; Dosani, T.; Kumar, A.; Seal, S.; Self, W. T. Cerium oxide nanoparticles scavenge nitric oxide radical (-NO). *Chem. Commun.* **2012**, *48*, 4896–4898.
- (41) Lee, S.; Van Remmen, H.; Csete, M. Sod2 overexpression preserves myoblast mitochondrial mass and function, but not muscle mass with aging. *Aging Cell* **2009**, *8*, 296–310.
- (42) Colon, J.; Hsieh, N.; Ferguson, A.; Kupelian, P.; Seal, S.; Jenkins, D. W.; Baker, C. H. Cerium oxide nanoparticles protect gastrointestinal epithelium from radiation-induced damage by reduction of reactive oxygen species and upregulation of superoxide dismutase 2. *Nanomed. Nanotechnol. Biol. Med.* **2010**, *6*, 698–705.
- (43) Nguyen, H. P.; Tran, P. H.; Kim, K. S.; Yang, S. G. The effects of real and simulated microgravity on cellular mitochondrial function. *npj Microgravity* **2021**, *7*, 44.
- (44) Nowaczyk, M.; Malcher, A.; Zimna, A.; Łabędź, W.; Kubaszewski, Ł.; Fiedorowicz, K.; Wierzbiński, K.; Rozwadowska, N.; Kurpisz, M. Transient and stable overexpression of extracellular superoxide dismutase is positively associated with the myogenic function of human skeletal muscle-derived stem/progenitor cells. *Antioxidants* **2020**, *9*, 817–819.